Crystal Growth and Magnetism of Transition Metal Pyrochlore Fluorides

Lakshani W. Masachchi, Navindra Keerthisinghe, Gregory Morrison, Anna A. Berseneva, Mark D. Smith, and Hans-Conrad zur Loye*

Department of Chemistry and Biochemistry, University of South Carolina, Columbia, SC, 29208, United States

*Corresponding author. E-mail: zurloye@mailbox.sc.edu

Abstract

Geometric magnetic frustration arises when the geometry of a structure prevents the simultaneous fulfillment of nearest-neighbor antiferromagnetic interactions and is commonly observed in lattices that exhibit a triangular topology, such as those found in the pyrochlore structure. *Via* a mild hydrothermal route, we have synthesized seven quaternary β-pyrochlore related fluorides $A_xM^{2+}{}_xM^{3+}{}_{(2-x)}F_6$, ($A$ = Cs and Rb; M^{2+} = Co^{2+}, Ni^{2+} and Zn^{2+}; and M^{3+} = V^{3+} and Fe^{3+}). Crystal structures and compositions were determined using a combination of single-crystal X-ray diffraction and energy-dispersive spectroscopy. After adjusting the reaction conditions, phase pure products of $A_xM^{2+}{}_xM^{3+}{}_{(2-x)}F_6$ were obtained. The magnetic susceptibility and isothermal magnetization data for all seven compounds were collected to interpret the magnetic behavior, which ranged from paramagnetic to antiferromagnetic with and without a ferromagnetic component. We found that the magnetic behavior of the $A_xM^{2+}{}_xV^{3+}{}_{(2-x)}F_6$ pyrochlore structures strongly depends on the presence or absence of unpaired electrons on the M^{2+} position. The titled pyrochlore compounds, with the exception of the Zn-analog, can be considered frustrated materials, with frustration indices in the range of 6 –13.

Introduction

The phenomenon of magnetic frustration has captured significant attention in recent years, encompassing a spectrum of exotic and degenerate magnetic ground states, such as spin glass, spin ice, and spin liquid.[1] The defining characteristic of magnetic frustration is the lack of magnetic order despite appreciable magnetic exchange coupling, which in the ideal case, can persist down to absolute zero temperature. This frustration primarily arises from the geometric configuration of the lattice, often featuring triangular or tetrahedral structure units with antiferromagnetic interactions that cannot all be satisfied simultaneously.[2–4] The ideal pyrochlore structure is denoted as $A_2M_2X_6Y$, where *A* and *M* are metal cations and *X* and *Y* are anions. *A* and *M* cations form two interpenetrating networks of corner-sharing tetrahedra, representing a quintessential framework for geometrically frustrated materials with magnetic ions occupying either the *A* or *M* sites.[1–4] Over the past few decades, a plethora of oxide pyrochlore materials have been reported and extensively investigated for their magnetic properties.[2,3,5] Magnetic ions contained in oxide pyrochlores are mostly limited to rare earth metals and some transition metals with higher oxidation states.[3] Increasingly, fluoride pyrochlores are drawing attention due to their ability to accommodate transition metals with low oxidation states, a feature that is not attainable with oxide pyrochlores.[4] Despite having different oxidation states, with fluoride being –1 and oxygen being –2, fluoride and oxide anions share similarities in their ionic radii ($r(O^{2-})$ =1.4 Å, $r(F^-)$ = 1.33 Å) and electronegativities (3.44 for O and 3.98 for F). Upon substituting divalent oxide (O^{2-}) with monovalent fluoride (F^-), the elemental composition must adjust to accommodate the lower anion charge, which can result in the formation of new materials that retain the pyrochlore structure.[4] Furthermore, the strong coupling of transition metals containing unpaired electrons favors the formation of magnetic interactions at accessible temperatures; this happens more so for transition metals rather than for rare earth metals.[6]

The initial report of polycrystalline products of fluoride pyrochlores dates back to 1970.[4] However, magnetic studies of these pyrochlores were conducted only recently, when the Cava group obtained large single crystals of $AA'M_2F_7$ type pyrochlores using the floating zone method.[6–8] Here, *A* denotes alkali elements and *A*' represents alkaline earth elements that are fully disordered, and *M* are transition metals. The result of these studies have shown that $NaA'M_2F_7$ materials (*A'* = Ca or Sr and *M* = Ni, Co, or Fe) display strong antiferromagnetic interactions with frustration indices ranging from 19-58,[6–9] where the frustration index $f = \theta_{CW} / T_C$, denotes the

strength of magnetic frustration based on the ratio of the Weiss temperature, θ_{CW}, to the transition temperature, T_C.[6] The level of frustration in a material can be estimated by the f value where, typically, when the frustration index f exceeds 10, the material is classified as being in a state of frustration.[10]

Geometrically frustrated magnetism can be observed in both ideal ($A_2M_2X_6Y$) and β-pyrochlore ($\square M_2X_6A$) materials. In β-pyrochlores, the A cations occupy the Y sites of the ideal pyrochlore ($A_2M_2X_6Y$) leaving vacancies at the original A crystallographic sites.[11,12,13] The displacement of the non-magnetic A cation does not affect the M cation network in β-pyrochlores. For fluoride pyrochlores, the ideal pyrochlore formula can be denoted as $A_2M_2F_6F'$, while the β-pyrochlores formula is $\square M_2F_6A$. In β-pyrochlores, mixed valent transition metals can occupy the M site and denoted as $\square M^{2+}M^{3+}F_6A$, or $AM^{2+}M^{3+}F_6$ as used in this manuscript. Typically, the cubic β-pyrochlores are disordered, where both M^{2+} and M^{3+} cations occupy the same site.[14] However, ordered orthorhombic structures have been reported with crystallographically ordered M^{2+} and M^{3+}cations.[15,16]

Previous studies have shown that orthorhombic pyrochlores, such as $CsFeFeF_6$ (f = 19), $RbFeFeF_6$ (f = 17), and $CsMnMnF_6$ (f = 4), exhibit lower magnetic frustration compared to their cubic counterparts, including $CsNiFeF_6$ (f = 37), $CsCoFeF_6$ (f = 54), and $CsMnFeF_6$ (f = 11).[14, 15,17–22] Therefore, we are interested in studying β-pyrochlores having cubic symmetry in order to test their magnetic frustration. The cubic pyrochlore compositions reported in the literature were obtained using the flux method, and some of the orthorhombic charge-ordered pyrochlores were synthesized using both flux and mild hydrothermal methods.[20,23] Although cubic $AM^{2+}M^{3+}F_6$ pyrochlores (A = Cs and Rb; M^{2+}=Co^{2+}, Ni^{2+}, and Mn^{2+}; and M^{3+} = Fe^{3+} and Cr^{3+}) have been studied for their magnetism, those with M^{3+} = V^{3+} remain unexplored. Even though some β-pyrochlores, such as $CsCoVF_6$, $CsNiVF_6$, $CsZnVF_6$, and $CsZnFeF_6$, have been reported previously, magnetic analyses for these materials are yet to be performed.[24–26] In order to identify the contribution of individual M^{2+} and M^{3+} cations toward frustration, it is necessary to synthesize additional compounds belonging to this family.

Herein we report the mild hydrothermal synthesis of seven β-pyrochlore related compounds. Compounds **1–6**, $Cs_{0.86}Co_{0.86}V_{1.14}F_6$, $Cs_{0.9}Ni_{0.9}V_{1.1}F_6$, $Cs_{0.9}Zn_{0.9}V_{1.1}F_6$, $CsZnFeF_6$, $Rb_{0.93}Co_{0.93}V_{1.07}F_6$, and $Rb_{0.97}Ni_{0.97}V_{1.03}F_6$, respectively, are disordered cubic while compound **7**,

$Rb(Zn_{0.2}V_{0.8})(Zn_{0.8}V_{0.2})F_6$, is a partially charged ordered orthorhombic phase. Their synthesis, crystal structures, and magnetic behaviors are discussed.

Experimental

Synthesis

Materials: RbCl (99.8%, Alfa Aesar), CsCl (99%, Alfa Aesar), CsF (99%, Alfa Aesar), V_2O_3 (95%, Alfa Aesar), $Fe(C_5H_7O_2)_3$ (99%, Stem), $Mn(CH_3COO)_2$•$4H_2O$ (98%, Alfa Aesar), $Ni(CH_3COO)_2$•$4H_2O$ (98%, Sigma-Aldrich), $Zn(CH_3COO)_2$•$2H_2O$ (98%, Fisher), $Co(CH_3COO)_2$•$4H_2O$ (98%, Alfa Aesar), and HF (49% aqueous, VWR®) were used as received. *Caution! Hydrofluoric acid is highly corrosive and acutely toxic and must be handled with proper safety precautions in a well-ventilated space. In case of exposure, proper treatment with immediate medical attention is essential.*

Using the mild hydrothermal synthesis,[15,16] seven mixed metal β-pyrochlore related fluorides with compositions $AM^{2+}VF_6$ (A = Cs and Rb; and M^{2+} = Ni^{2+}, Co^{2+}, and Zn^{2+}) and $CsZnFeF_6$ were successfully synthesized. The starting materials (Table 1) were added to a 23 mL PTFE liner along with 1 mL of deionized water and 1 mL of 49% aqueous HF and sealed in a steel autoclave. The autoclave was heated to 200 °C at 10 °C/min in a programmable convection oven, allowed to dwell for 12 hours, and cooled to room temperature by shutting off the oven. The polycrystalline powders were isolated *via* vacuum filtration and washed with methanol and acetone. Following this, the isolated products were sonicated for 30 minutes in methanol, and the final products were collected by vacuum filtration.

Table 1. Starting Reagents for pyrochlore synthesis.

	Chemical Formula	$M(CH_3COO)_2$ •$4H_2O$ (mmol)	V_2O_3(mmol)/ $Fe(C_5H_7O_2)_3$ (mmol)	ACl (mmol)	AF (mmol)	49% HF (mL)	H_2O (mL)
1	$Cs_{0.86}Co_{0.86}V_{1.14}F_6$	2	1	2	0	1	1
2	$Cs_{0.9}Ni_{0.9}V_{1.1}F_6$	2	1	2	0	1	1
3	$Cs_{0.9}Zn_{0.9}V_{1.1}F_6$	2	1	2	0	1	1
4	$CsZnFeF_6$	2	2	0	2	1	1

5	$Rb_{0.93}Co_{0.93}V_{1.07}F_6$	4	2	4	0	1	1
6	$Rb_{0.97}Ni_{0.97}V_{1.03}F_6$	4	2	4	0	1	1
7	$Rb(Zn_{0.2}V_{0.8})(Zn_{0.8}V_{0.2})F_6$	4	1	4	0	1	1

Single-Crystal X-ray Diffraction (SXRD)

X-ray intensity data were collected at 298(2) or 301(2) K using a Bruker D8 QUEST diffractometer equipped with a PHOTON-II area detector and an Incoatec microfocus source (Mo Kα radiation, λ = 0.71073 Å). The crystals were mounted on a microloop using immersion oil. The raw area detector data frames were reduced and corrected for absorption effects using the SAINT+ and SADABS programs.[27,28] Final unit cell parameters were determined by least-squares refinement. Initial structural models were obtained with SHELXT.[29] Subsequent difference Fourier calculations and full-matrix least-squares refinement against F^2 were performed with SHELXL-2018 using Olex2. The crystallographic data and results of the diffraction experiments are summarized in Table 2.

Powder X-ray Diffraction (PXRD)

Powder X-ray diffraction data were collected on a Bruker D2 Phaser powder X-ray diffractometer using Cu Kα radiation to confirm the phase purity of polycrystalline samples obtained by grinding single crystals (Figure S1 and S2). The data were collected between the angular range 5–65° 2θ in step of 0.04° over 60 minutes.

Energy-Dispersive Spectroscopy (EDS)

EDS was performed on single crystals using a TESCAN Vega-3 SBU scanning electron microscope (SEM) with a Thermo EDS attachment operated in low-vacuum mode (Table S1). The crystals were mounted on an SEM stub with carbon tape and analyzed using 20 kV accelerating voltage and an accumulation time of 20 seconds.

Magnetic Measurements

Susceptibility and magnetization measurements were performed on ground single crystals using a Quantum Design MPMS3 SQUID magnetometer. Susceptibility measurements were collected

under zero-field cooled (ZFC) and field-cooled (FC) conditions in the temperature range of 2−300 K at an applied field of 0.1 T. Magnetization as a function of the field was measured at 2 K in an applied field ranging from −5 to +5 T. The raw data were corrected for radial offset and shape effects.[30] AC measurements were performed on $Cs_{0.86}Co_{0.86}V_{1.14}F_6$ at applied field 0.025 Oe with a frequency of 100, 200, 500, and 1000 Hz (Figure S12) to further study the magnetic transition.

Inductively coupled plasma optical emission spectroscopy (ICP-OES)

ICP-OES was performed using a Perkin Elmer Avio 200 spectrometer on digested samples of $Cs_{0.9}Zn_{0.9}V_{1.1}F_6$ and $Rb(Zn_{0.2}V_{0.8})(Zn_{0.8}V_{0.2})F_6$. The digestion was performed in PerkinElmer's Titan MPS Microwave Sample Preparation System. The crystalline sample (≈ 2.0 mg) was loaded into a Teflon liner with 8 mL of aqua regia (HNO_3, HCl, and deionized water were mixed in a 4:8:3 volume ratio). The Teflon liner was placed into a programmable microwave oven. The oven was ramped to 175 °C and 30 bars in 30 min. The sample was held at that temperature and pressure for 10 minutes and cooled down to 50 °C in 125 min. Once at room temperature, the digested sample was diluted to the appropriate concentrations using 5 wt % HNO_3. The calibration curves were measured for Zn and V by axial detector (Table S4).

Electron paramagnetic resonance (EPR) measurements

EPR measurements were carried out on a Bruker EMX plus equipped with a Bruker X-band microwave bridgehead and Xenon software (v 1.2). Solid samples were loaded into quartz tubes. All spectra were recorded at room temperature and a microwave frequency of 9.705 GHz.

Results and Discussion

Synthesis

The mild hydrothermal synthesis method is convenient for preparing many fluoride materials, which motivated us to use this approach to target the synthesis of new compositions of β-pyrochlore fluorides.[15,31–33] Single crystals along with polycrystalline powders of $AM^{2+}M^{3+}F_6$ (A = Cs and Rb; M^{2+} = Co^{2+}, Ni^{2+}, and Zn^{2+}; and M^{3+} = V^{3+} and Fe^{3+}) were successfully obtained hydrothermally using HF as a fluorinating agent and as a solvent at the relatively low temperature of 200°C. The conditions were adjusted after several trial syntheses to obtain phase-pure single-crystal products. The desired target products were obtained by varying starting reagents and their ratios and concentrations, HF and water volume ratio, and temperature profiles. The initial reagent ratios were selected according to the stoichiometry of the desired product (Table 1) with 1 mmol of M^{2+} and 1 mmol of M^{3+} being used. However, for $Rb(Zn_{0.2}V_{0.8})(Zn_{0.8}V_{0.2})F_6$, a phase pure product was obtained only when the starting reagent atomic ratio of M^{2+}:M^{3+} was 2:1. Using $FeCl_3$•$6H_2O$ and CsCl as starting reagents for $CsZnFeF_6$ resulted in a mixed-valent iron phase $CsFe^{2+}Fe^{3+}F_6$. The Fe^{2+} component results from the *in-situ* reduction of Fe^{3+}, which is facilitated by the oxidation of Cl^-.[15] Therefore, CsF and $Fe(C_5H_7O_2)_3$ were used to grow $CsZnFeF_6$ crystals. Exploring the use of different volume ratios of HF to H_2O resulted in many different ternary and quaternary phases, some known and some new, which will be described in a separate paper. Only a 1:1 volume ratio of HF:H_2O led to the pure phases of β-pyrochlore related fluorides, while a deviation from this ratio resulted in the formation of other phases. Additional experiments demonstrated that changing the reaction temperature, dwell time, and slow cooling did not improve the crystal quality. However, a slow heating rate (0.1°C/min), when compared to fast heating (10°C/min), resulted in the formation of much larger crystals. Finally, sonicating the polycrystalline products with methanol results in the selective dissolution of the binary fluoride impurities as well as of any remaining starting reagents, allowing the isolation of the pure target phase.

Table 2. Crystallographic data for **1**-**7**.

	(1) $Cs_{0.86}Co_{0.86}V_{1.14}F_6$	**(2)** $Cs_{0.9}Ni_{0.9}V_{1.1}F_6$	**(3)** $Cs_{0.9}Zn_{0.9}V_{1.1}F_6$	**(4)** $CsZnFeF_6$	**(5)** $Rb_{0.93}Co_{0.93}V_{1.07}F_6$	**(6)** $Rb_{0.97}Ni_{0.97}V_{1.03}F_6$	**(7)** $Rb(Zn_{0.2}V_{0.8})(Zn_{0.8}V_{0.2})F_6$
Formula weight	337.58	342.11	348.67	364.09	302.75	305.90	315.78
Temperature, K	298(2)	301(2)	298(2)	298(2)	301(2)	301(2)	298(2)
Crystal system	cubic						orthorhombic
Space group, Z	*F d -3 m,* 8						*Pnma,* 4
a, Å	10.3892(2)	10.3165(6)	10.3713(10)	10.4178(12)	10.32480(12)	10.25360(17)	7.0931(4)
b, Å							7.3406(4)
c, Å							10.1337(5)
Volume, $Å^3$	1121.36(7)	1098.0(2)	1115.58(3)	1130.65(4)	1100.64(4)	1078.03(5)	527.64(5)
ρ_{calc}, g/cm^3	3.999	4.139	4.152	4.278	3.654	3.770	3.975
μ/mm^{-1}	10.008	10.853	11.546	12.732	12.820	13.861	15.517
F(000)	1208	1231	1240	1307	1105	1124	576
Crystal size, mm^3	0.090 × 0.080 × 0.060	0.020 × 0.010 × 0.010	0.080 × 0.060 × 0.007	0.080 × 0.070 × 0.05	0.140 × 0.100 × 0.080	0.070 × 0.060 × 0.040	0.052 × 0.030 × 0.012
Radiation (λ, Å)	Mo k_α (0.71073)						
2θ range, deg.	6.792 – 59.74	6.840 – 65.104	6.804 – 72.668	6.774 – 72.432	6.836 – 69.752	6.882 – 68.544	6.854 – 72.616
Reflections collected	2328	6101	31509	5791	7542	10436	40395
Data/restraints/ parameters	102/0/10	123/1/11	162/2/14	164/0/11	146/0/15	136/0/13	1339/0/50
Goodness-of-fit	1.183	1.262	1.325	1.186	1.125	1.078	1.126
R_1 [I>=2σ (I)]	0.0199	0.0245	0.0113	0.0132	0.0188	0.0203	0.0259
wR_2 [all data]	0.0394	0.0419	0.0353	0.0300	0.0521	0.0430	0.0507
Largest diff. peak/hole, e $Å^{-3}$	0.82/–0.57	0.493/–0.460	0.34/–0.24	0.48/–0.40	0.473/–0.520	0.654 /–0.658	1.27/–1.54
R_{int}, %	3.10	4.23	4.85	5.17	3.84	3.50	4.05

Crystal Structure Description

The $A_xM^{2+}{}_xM^{3+}{}_{(2-x)}F_6$ compounds (**1**-**6**) crystalize in the cubic space group *Fd*-3*m*, while **7**, $Rb(Zn_{0.2}V_{0.8})(Zn_{0.8}V_{0.2})F_6$, crystallizes in the orthorhombic space group *Pnma*. $Rb_{0.97}Ni_{0.97}V_{1.03}F_6$, $Rb_{0.93}Co_{0.93}V_{1.07}F_6$, and $Rb(Zn_{0.2}V_{0.8})(Zn_{0.8}V_{0.2})F_6$ are new members of the $RbNiCrF_6$ structure type. The compositions and structures of $CsCoVF_6$, $CsNiVF_6$, $CsZnVF_6$, and $CsZnFeF_6$ structures have been previously reported as stoichiometric phases.[24–26] However, they differ from our single crystal structure determinations of **1-3**, $Cs_{0.86}Co_{0.86}V_{1.14}F_6$, $Cs_{0.9}Ni_{0.9}V_{1.1}F_6$, and $Cs_{0.9}Zn_{0.9}V_{1.1}F_6$, that do not refine to full site occupancies, although the structures are otherwise the same.

The three-dimensional framework of the β-pyrochlore structure consists primarily of $M^{2+}/M^{3+}F_6$ corner-sharing octahedra with pores filled by the *A* cations. The cubic pyrochlore compositions (**1**-**6**) are isostructural and represent a disordered system as both transition metals occupy the same crystallographic site, a requirement for cubic symmetry. The $M^{2+}/M^{3+}F_6$ octahedra of the cubic β-pyrochlore structure are regular octahedra and have six identical *M*–F bond lengths and 90° F–*M*–F angles (Figure 1). Site disorder and less than full occupancy of the *A* cation site (*A* = Cs/Rb) are observed in the cubic pyrochlore materials, (**1**-**6**), reported herein. Structure refinements resulted in improved refinement parameters for all structures when the Cs/Rb occupancy is linked with the site occupancy of M^{2+} and M^{3+} to maintain charge balance, i.e., the $A_xM^{2+}{}_xM^{3+}{}_{(2-x)}F_6$ compositions. The resultant refinement of the M^{2+} and M^{3+} site occupancies deviates from an exact 50:50 ratio, which results in this series of nonstoichiometric compounds (Table S2).

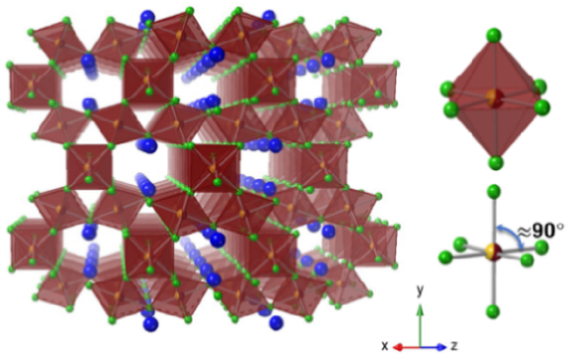

Figure 1. View of cubic β-pyrochlore crystal structure (brown octahedra represent the $M^{2+}/M^{3+}F_6$, Cs/Rb, and F atoms in blue and green spheres, respectively) and the individual coordination environment of M^{2+}/M^{3+} site in cubic pyrochlores.

The crystal structure of the orthorhombic $Rb(Zn_{0.2}V_{0.8})(Zn_{0.8}V_{0.2})F_6$ phase contains two crystallographically unique octahedral positions that exhibit anti-site mixing of M^{2+} and M^{3+}. The $(Zn_{0.2}V_{0.8})F_6$ coordination environment is nearly octahedral, with bond distances and bond angles falling into the ranges of 1.911–1.935 Å and 88–92°, respectively. By contrast, the $(Zn_{0.8}V_{0.2})F_6$ octahedron exhibits a distortion resulting from four longer bonds (2.034–2.049 Å) and two shorter bonds (1.944 Å and 1.969 Å) and bond angles ranging from 82 to 109° (Figure 2). The anti-site mixing in $Rb(Zn_{0.2}V_{0.8})(Zn_{0.8}V_{0.2})F_6$ leads to partial metal site ordering, which results in the orthorhombic symmetry of the material.

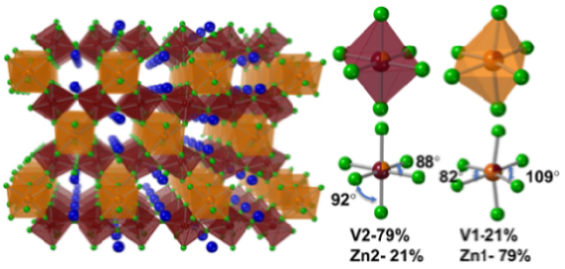

Figure 2. View of orthorhombic pyrochlore crystal structure (brown and yellow octahedra represent $(Zn_{0.2}V_{0.8})F_6$ and $(Zn_{0.8}V_{0.2})F_6$ sites) and the individual coordination environments of $Rb(Zn_{0.2}V_{0.8})(Zn_{0.8}V_{0.2})F_6$.

Magnetic Properties

The $M^{2+}F_6$ and $M^{3+}F_6$ polyhedra in the cubic and orthorhombic pyrochlore structures are arranged into a corner-sharing tetrahedral arrangement shown in Figure 3a. As a result, each M^{2+}/M^{3+} site is associated with three Kagome layers. The three Kagome layers in the cubic pyrochlore structure are identical and consist of equilateral triangles (Figure 3b); on the other hand, the Kagome layers of the orthorhombic pyrochlore structure are different in that two of them consist of isosceles triangles (Figure 3c) and one is comprised of scalene triangles (Figure 3d). When these M^{2+}/M^{3+} sites are occupied with magnetic cations, it leads to geometrically frustrated magnetism.[4,14,15] To investigate the magnetic behavior of the title compounds, we collected zero field-cooled and field-cooled DC magnetic susceptibility vs. temperature and magnetization vs. field data, the results of which are summarized in Table 3.

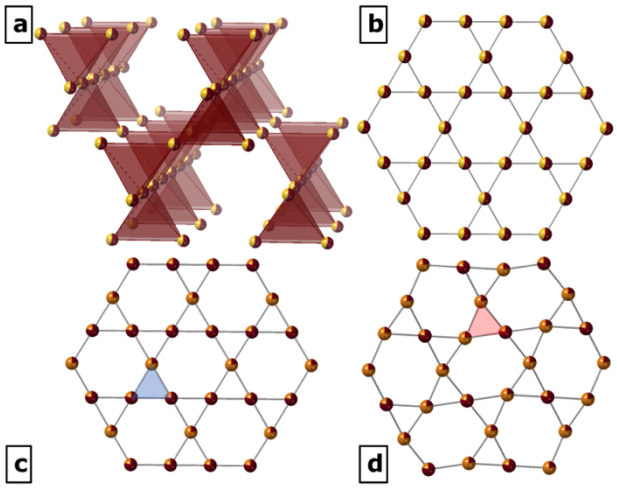

Figure 3. The view of the corner-shared tetrahedral arrangement of magnetic ions (a) and Kagome layer of cubic pyrochlore (b). Representation of Kagome layer with blue color isosceles triangles (c) Kagome layer with red color scalene triangles (d) of orthorhombic pyrochlore.

Table 3. Magnetic Properties of **1**–**7**.

Chemical Formula	Magnetic Properties	Effective magnetic moment (μ_{eff}) (μ_B/F.U.)		θ_{CW} (K)	Magnetic ordering T (K)	Frustration Index
		observed	calculated			
$Cs_{0.9}Zn_{0.9}V_{1.1}F_6$	paramagnetic	2.02	2.97	–9	-	-
$Rb(Zn_{0.2}V_{0.8})(Zn_{0.8}V_{0.2})F_6$	paramagnetic	1.94	2.83	1	-	-
$Cs_{0.86}Co_{0.86}V_{1.14}F_6$	antiferromagnetic	5.50	4.69	–54	8	7
$Cs_{0.9}Ni_{0.9}V_{1.1}F_6$	antiferromagnetic	3.91	4.00	–63	5	13
$Rb_{0.97}Ni_{0.97}V_{1.03}F_6$	antiferromagnetic	3.87	4.00	–58	6	10
$Rb_{0.93}Co_{0.93}V_{1.07}F_6$	antiferromagnetic	5.18	4.74	–49	8	6
$CsZnFeF_6$	antiferromagnetic	6.30	5.92	–217	-	-

Magnetic susceptibility and inverse susceptibility as a function of temperature plots are shown in Figure 4. The high-temperature regions (150 to 300 K) of the plots were fit to the Curie-Weiss law $\chi = \frac{C}{T-\theta_{CW}}$, where χ is the magnetic susceptibility, C is the Curie constant, T is temperature, and θ_{CW} is the Weiss temperature.[15,33] Both cobalt-containing compounds ($Cs_{0.86}Co_{0.86}V_{1.14}F_6$ and $Rb_{0.93}Co_{0.93}V_{1.07}F_6$) have an experimental magnetic moment that is larger than the spin-only moment, presumably due to spin-orbital coupling of Co^{2+}.[33] For $Cs_{0.9}Zn_{0.9}V_{1.1}F_6$, and $Rb(Zn_{0.2}V_{0.8})(Zn_{0.8}V_{0.2})F_6$, notably reduced experimental magnetic moments are observed when compared to the calculated moments (Table 3). In previous literature reports, this discrepancy is reported for V^{3+}-compounds and is explained by the contribution of spin-spin coupling or spin-orbital coupling to the overall magnetic moment.[34,35] To confirm the reduced moment of V^{3+} in these samples, a second sample of each was prepared and it's magnetic properties measured. Furthermore, we performed inductively coupled plasma optical emission spectroscopy (ICP-OES) for both of these samples and confirmed the formula derived from SXRD (see SI for more information, Table S4). Finally, to address the oxidation state of vanadium in $Cs_{0.9}Zn_{0.9}V_{1.1}F_6$ and $Rb(Zn_{0.2}V_{0.8})(Zn_{0.8}V_{0.2})F_6$ compounds, we conducted electron paramagnetic resonance (EPR) measurements. For both samples, we observed an EPR single in the X-band, which was well-refined ($R^2 > 0.995$) with only one Lorentz derivative profile, and multi-component fitting did not improve fitting characteristics (Figures S10 and S11). Therefore, SXRD, ICP-OES, and EPR support the formulas of $Cs_{0.9}Zn_{0.9}V^{3+}{}_{1.1}F_6$ and $Rb(Zn_{0.2}V^{3+}{}_{0.8})(Zn_{0.8}V^{3+}{}_{0.2})F_6$ and that the reduced magnetic moments in these compounds are a feature of V^{3+}.

Both $Cs_{0.9}Zn_{0.9}V_{1.1}F_6$ and $Rb(Zn_{0.2}V_{0.8})(Zn_{0.8}V_{0.2})F_6$ exhibit only paramagnetic behavior and do not exhibit a magnetic transition down to 2 K (Figures 4a and 4b). However, a magnetic transition is evident in all the other vanadium compounds, ($Cs_{0.86}Co_{0.86}V_{1.14}F_6$, $Cs_{0.9}Ni_{0.9}V_{1.1}F_6$, $Rb_{0.97}Ni_{0.97}V_{1.03}F_6$, and $Rb_{0.93}Co_{0.93}V_{1.07}F_6$), in the very low-temperature region as illustrated in Figures 4c–4f, respectively. This highlights that in order for the V^{3+}-containing β-pyrochlores to exhibit magnetic order it is necessary to have cations with unpaired electrons on the M^{2+} site.

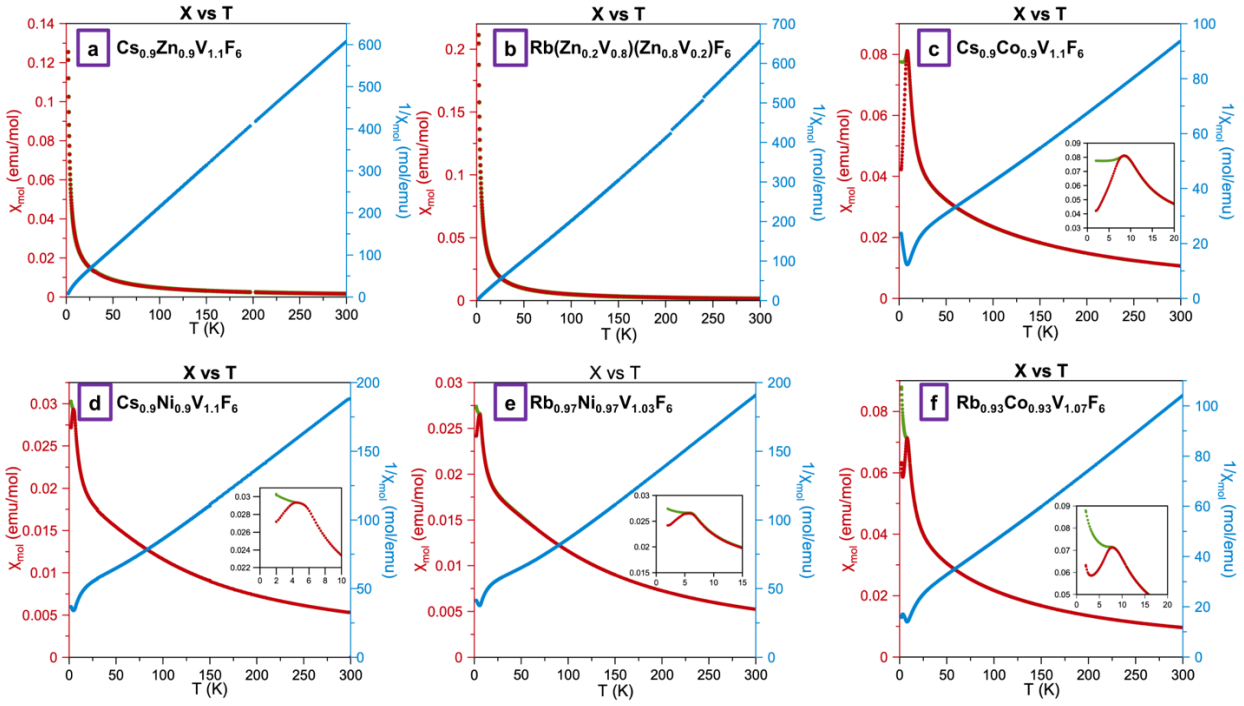

Figure 4. DC molar magnetic susceptibility (χ_{mol}) and inverse susceptibility ($1/\chi_{mol}$) vs. temperature plots for compounds **1**-**6**. Zero-field-cooled data are shown in red, field-cooled data in green, and inverse susceptibility data in blue. Full-scale magnetism plots for each material are provided in Figures S3−S9 in the Supporting Information.

The large negative Weiss temperatures of $Cs_{0.86}Co_{0.86}V_{1.14}F_6$, $Cs_{0.9}Ni_{0.9}V_{1.1}F_6$, $Rb_{0.93}Co_{0.93}V_{1.07}F_6$, and $Rb_{0.97}Ni_{0.97}V_{1.03}F_6$ (–49 K to –63 K), indicate strong antiferromagnetic interactions in these materials (Table 3).[36] It is worth pointing out that $CsZnFeF_6$ is an outlier when compared to the vanadium compounds. As shown in Figure 5, no long-range magnetic transition is evident down to 2K. Nonetheless, a large negative Curie−Weiss temperature (–217 K) is observed for $CsZnFeF_6$, indicative of stronger antiferromagnetic interactions when compared to the vanadium analogs. The reported Weiss temperatures (θ_{CW}) for the known β-pyrochlores, such as $CsNiFeF_6$, $CsCoFeF_6$, $CsMnFeF_6$, $CsNiCrF_6$, $CsCoCrF_6$, $CsMnCrF_6$, and $CsFeCrF_6$, are –210 K, –240 K , –300 K, –70 K, –76 K, –68 K, and –98 K, respectively (Table 4).[17–19,22] According to Goodenough, the Weiss temperature in β-pyrochlores represents the sum of the nearest-neighbor interactions between the magnetic ions, as per his superexchange rules.[18,37] Due to the random distribution of magnetic ions on the M^{2+}/M^{3+} site, there will be interactions involving the cations pairs (M^{2+}–M^{3+}), (M^{2+}–M^{2+}), and (M^{3+}–M^{3+}).[18,22] According to the Berkooz *et.al*,[18] a moderate ferromagnetic contribution for the interaction (M^{2+}–F–M^{3+}), a weak antiferromagnetic contribution

for the interaction (M^{3+}–F–M^{3+}), and a strong antiferromagnetic contribution (M^{2+}–F–M^{2+}), were suggested for the β-pyrochlore compounds that contain ion pairs (Fe^{2+}, V^{3+}), (Mn^{2+}, Cr^{3+}) and (Fe^{2+}, Cr^{3+}). Also, all nearest neighbor interactions within $CsM^{2+}Fe^{3+}F_6$ (M^{2+} = Ni^{2+} and Mn^{2+}) compounds are predicted to be strongly antiferromagnetic.[18] Thus, for the Cr^{3+} and V^{3+} compounds, (M^{2+}–F–M^{3+}) interactions should be moderately ferromagnetic, thus reducing the negative value of θ_{CW} compared to the $CsM^{2+}Fe^{3+}F_6$ compounds where all the magnetic interactions are antiferromagnetic.[18] Moreover, the known inverse weberite compounds also exhibited higher Weiss temperatures for $M^{2+}Fe^{3+}F_5(H_2O)_2$ compared to $M^{2+}Cr^{3+}F_5(H_2O)_2$, and $M^{2+}V^{3+}F_5(H_2O)_2$, where M^{2+} is Ni^{2+}/Co^{2+}: e.g., $CoFeF_5(H_2O)_2$, $CoCrF_5(H_2O)_2$, $NiCrF_5(H_2O)_2$, and $NiVF_5(H_2O)_2$, θ_{CW} is equal to –175 K, –46 K, –56 K, and –56 K, respectively (Table 4).[33] We therefore suggest that, based on the type of interaction present between (M^{2+}–F–M^{3+}), the magnitude of the Weiss temperature can be estimated. If M^{2+}–F–M^{3+} exhibits a ferromagnetic component, the negative value of the Weiss temperature will be reduced, and if the interaction between M^{2+}–F–M^{3+} is antiferromagnetic, the negative value of the Weiss temperature will be further increased. According to the Kanamori−Goodenough rules, the 180° superexchange interactions between the same kind of cations in octahedral sites generally exhibit antiferromagnetic interaction (180° cation-anion-cation superexchange rule also applies to the ~139° interactions, Table S3).[37]

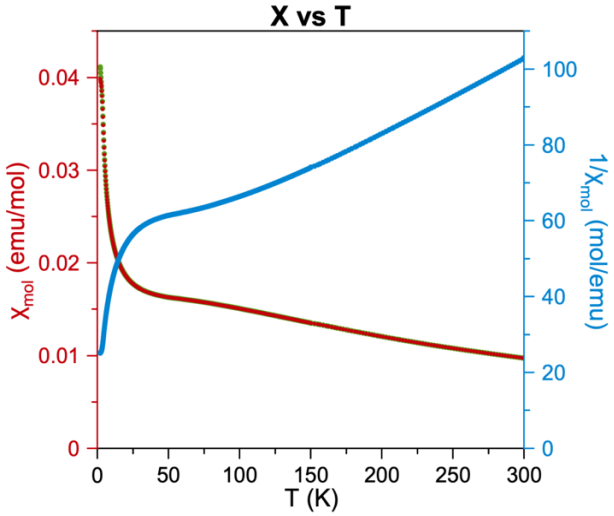

Figure 5. Magnetic susceptibility and inverse magnetic susceptibility for the temperature range 2−300 K of $CsZnFeF_6$. Zero-field-cooled data are shown in red, and field-cooled data are shown in blue.

Table 4. Magnetic data for previously reported pyrochlores, β-pyrochlores, weberites and inverse weberites. (pyrochlore; P, β-pyrochlore; BP, weberite; W, inverse weberite; IW, cubic; *c*, orthorhombic; *o*).

Compound	Structure type	Unpaired electrons		θ_{CW}(K)	Magnetic ordering T (K)	Frustration Index (f
		M^{2+}	M^{3+}			
$CsNiFeF_6$[17, 19]	BP (*c*)	2	5	–210	5	37
$CsCoFeF_6$[19]	BP (*c*)	3	5	–240	4.4	54.5
$CsMnFeF_6$[17]	BP (*c*)	5	5	–300	27	11
$CsNiCrF_6$[22]	BP (*c*)	2	3	–70	3	23
$CsCoCrF_6$[19]	BP (*c*)	3	3	–76	3.4	22
$CsMnCrF_6$[18]	BP (*c*)	5	3	–67	-	-
$CsFeCrF_6$[18]	BP (*c*)	4	3	–98	5	20
$CsFeFeF_6$[21]	BP (*c*)	4	5	–260	14	19
$RbFeFeF_6$[20]	BP (*o*)	4	5	–270	16	17
$CsMnMnF_6$[15]	BP (*o*)	5	4	–93.7	24	4
$NaSrCo_2F_7$[8]	P	3	0	–127	3	42
$NaCaCo_2F_7$[6]	P	3	0	–140	2.4	56
$NaCaNi_2F_7$[7]	P	2	0	–129	3.6	36
$NaSrMn_2F_7$[9]	P	5	0	–89.7	2.5	35.9
$NaSrFe_2F_7$[9]	P	4	0	–98.1	3.7	26.5
$NaCaFe_2F_7$[9]	P	4	0	–72.8	3.9	18.7
$NiVF_5(H_2O)_2$[33]	IW	2	1	–56.3	13.5	4.2
$CoCrF_5(H_2O)_2$[33]	IW	3	3	–46.5	5.7	8.1
$NiCrF_5(H_2O)_2$[33]	IW	2	3	–56.3	7.7	7.3
$MnCrF_5(H_2O)_2$[33]	IW	5	3	–24.1	3.5	6.9
$ZnCrF_5(H_2O)_2$[33]	IW	0	3	–33.4	15.5	2.3
$CoFeF_5(H_2O)_2$[33]	IW	2	5	–174.7	26.3	6.6
$MnFeF_5(H_2O)_2$[38]	IW	5	5	–267	39	6.7
$Fe_2F_5(H_2O)_2$[39]	IW	4	5	–256.8	48	5.3
Na_2CoCrF_7[40]	W	3	3	–107	2.9	7.3
Na_2CoFeF_7[40]	W	3	5	–100	80	1.3

Based on the Cava group analysis, rearranging the Curie−Weiss law $\chi = C/(T - \theta_{CW})$ to $C/(\chi|\theta_{CW}|) = T/|\theta_{CW}| - 1$, can be used to create a normalized, dimensionless plot that is useful for comparing magnetic behavior of different compounds.[8,9] In Figure 6 ideal antiferromagnets should follow the line $y = x + 1$ (shown as a dashed line in black), with the indications of magnetic ordering on the order of $\frac{T}{\theta_{CW}} \approx 1$. Deviations from the ideal antiferromagnetic behavior are observed for $Cs_{0.86}Co_{0.86}V_{1.14}F_6$, $Cs_{0.9}Ni_{0.9}V_{1.1}F_6$, $Rb_{0.97}Ni_{0.97}V_{1.03}F_6$, $Rb_{0.93}Co_{0.93}V_{1.07}F_6$, and

$CsZnFeF_6$, where positive or negative deviations from the dashed line imply the presence of excess antiferromagnetic or ferromagnetic correlations, respectively.[8,9] All five compounds follow the ideal Curie−Weiss behavior at high temperatures. Slight deviations are observed for $Cs_{0.86}Co_{0.86}V_{1.14}F_6$, $Cs_{0.9}Ni_{0.9}V_{1.1}F_6$, $Rb_{0.97}Ni_{0.97}V_{1.03}F_6$, and $Rb_{0.93}Co_{0.93}V_{1.07}F_6$ starting around $2.8T/\theta_{CW}$. At $0.3T/\theta_{CW}$, both $Cs_{0.86}Co_{0.86}V_{1.14}F_6$ and $Rb_{0.93}Co_{0.93}V_{1.07}F_6$ begin to deviate with a ferromagnetic correlation that increases as they approach their transition temperature. Conversely, strong antiferromagnetic deviations can be observed near $0.3T/\theta_{CW}$ for $Cs_{0.9}Ni_{0.9}V_{1.1}F_6$ and $Rb_{0.97}Ni_{0.97}V_{1.03}F_6$, which decrease as the transition temperature is approached. ($0.08T/\theta_{CW}$ and $0.10T/\theta_{CW}$, respectively). This illustrates that vanadium compounds with cobalt and nickel analogs experience significant and slight ferromagnetic correlation, respectively, around the transition temperature. Also, a significant antiferromagnetic deviation can be noticed in $CsZnFeF_6$. This data also supports the prediction of Berkooz *et.al* and confirms that all the nearest-neighbor interactions of Fe^{3+} compounds are antiferromagnetic, while the compounds containing V^{3+} include a ferromagnetic term for the nearest-neighbor interaction.[18] Moreover, zero field cooled and field cooled splitting in the susceptibility plots of $Cs_{0.86}Co_{0.86}V_{1.14}F_6$, $Cs_{0.9}Ni_{0.9}V_{1.1}F_6$, $Rb_{0.97}Ni_{0.97}V_{1.03}F_6$, and $Rb_{0.93}Co_{0.93}V_{1.07}F_6$, imply the presence of a ferromagnetic component, such as canted antiferromagnetic behavior, in these materials (Figure 4).[15] This discrepancy is more pronounced for $Cs_{0.86}Co_{0.86}V_{1.14}F_6$ and $Rb_{0.93}Co_{0.93}V_{1.07}F_6$ (Figure 4c and 4f, respectively), and hysteresis is observed in the M vs. H plots, shown in Figures S3 and S7. Thus, it appears that the ferromagnetic interaction between Co^{2+} and V^{3+} is more prominent than between Ni^{2+} and V^{3+}. To test for the presence of spin glass behavior we performed AC measurements on $Cs_{0.86}Co_{0.86}V_{1.14}F_6$ and did not observe a shift in the peak as a function of frequency, suggesting that no spin glass behavior is present. (Figure S12).

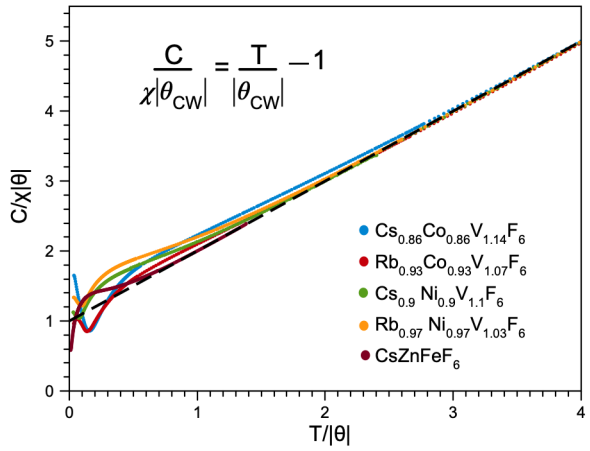

Figure 6. A dimensionless, normalized plot of the magnetization, comparing the behavior of $Cs_{0.9}Co_{0.9}V_{1.1}F_6$, $Cs_{0.9}Ni_{0.9}V_{1.1}F_6$, $Rb_{0.97}Ni_{0.97}V_{1.03}F_6$, $Rb_{0.93}Co_{0.93}V_{1.07}F_6$ and $CsZnFeF_6$ at temperatures near θ_{CW} and below. This is done by arranging the Curie–Weiss Law to $C/(\chi|\theta_{CW}|) = T/|\theta_{CW}| - 1$.

Magnetic Frustration

The frustration indices of the title compounds $Cs_{0.86}Co_{0.86}V_{1.1}F_6$, $Cs_{0.9}Ni_{0.9}V_{1.1}F_6$, $Rb_{0.97}Ni_{0.97}V_{1.03}F_6$, and $Rb_{0.93}Co_{0.93}V_{1.07}F_6$ fall into the range of 6−13 (Table 3). Typically, a frustration index larger than 10 implies a frustrated material.[7,8] We cannot determine a frustration index for $CsZnFeF_6$ as we could not observe a long range magnetic transition for $CsZnFeF_6$ down to 2 K. Very low-temperature magnetic susceptibility studies can be conducted as a future investigation to reveal the magnetic ordering temperature of $CsZnFeF_6$ and its magnetic behavior. Using data from the literature, we also estimated the frustration indices for known β-pyrochlores $CsNiFeF_6$, $CsCoFeF_6$, $CsNiCrF_6$, and $CsCoCrF_6$ $|f|$ to be equal to 37, 54, 23, and 22, respectively (Table 4),[17–19,22] which highlight that the frustration indices for Cr^{3+} and Fe^{3+} containing cubic β-pyrochlores are higher compared to $Cs_{0.9}Ni_{0.9}V_{1.1}F_6$ and $Cs_{0.9}Co_{0.9}V_{1.1}F_6$ where the $|f|$ is equal to 13 and 7, respectively (Table 3).

As mentioned earlier, the triangular topology may cause geometric frustration within the materials. In addition to pyrochlores, other structure types, such as weberite, and inverse weberite, exhibit a specific triangular topology, which results in magnetic frustration in these materials. Weberite fluorides have the general formula of $AM^{2+}M^{3+}F_7$ (A is an alkali metal, and M^{2+} and M^{3+}

are 3*d* metal cations), which is similar to the formula of fluoride pyrochlore. However, both M^{2+} and M^{3+} cations in the weberite structure reside on distinct octahedral sites where each vertex of the M^{2+} octahedron connects to another four M^{2+} octahedra and two M^{3+} octahedra, while only four vertices of M^{3+} octahedra link to other M^{2+} octahedra.[41] This connectivity of magnetic ions creates two separate Kagome layers within the weberite structure.[33] The inverse weberite ($M^{2+}M^{3+}F_5(H_2O)_2$) has a structure similar to weberites, with the exception that the M^{2+} and M^{3+} octahedral sites are switched, that two F atoms are replaced by water molecules, and the absence of *A* cations.[33,39,40] In general, the frustration indices of these compounds are less than 10 (Table 4), which indicates that pyrochlores are more magnetically frustrated compared to weberites and inverse weberites, as each magnetic cation belongs to three Kagome layers due to the corner-shared tetrahedral arrangement of magnetic ions in pyrochlores. By contrast, for weberite and inverse weberite, a magnetic cation is a part of only one or two Kagome layers.[15,33,39,40] Known orthorhombic charge-ordered $CsFe^{2+}Fe^{3+}F_6$ and $RbFe^{2+}Fe^{3+}F_6$ pyrochlores result in frustration indices of 19 and 17, respectively, which indicate low frustration compared to the disordered $CsNiFeF_6$ (f =37) and $CsCoFeF_6$ (f =54.5), even though their Weiss temperatures are closer to each other.[15,20,21] Cubic to orthorhombic structure changes can influence the less homogenous exchange interactions between magnetic ions, which lead to a more ordered magnetic structure with fewer competing interactions and less frustration. This suggests that the frustration index is decreasing in going from the cubic pyrochlore to the orthorhombic pyrochlore to the inverse weberite and to the weberite structure.

This study shows the significance of having cations with unpaired electrons on the M^{2+} site for the V^{3+}-containing β-pyrochlores to induce magnetic order and magnetic frustration within the materials. Nearest neighbor interactions between ions pairs also affect the Weiss temperature of the material; herein we suggest that the emergence of ferromagnetic interaction between (M^{2+}–F–V^{3+}) can reduce the Weiss temperature of V^{3+}-containing β-pyrochlores compared to the Fe^{3+}-based analogs. However, more compounds of this family need to be synthesized and studied to draw more definitive conclusions about the effect of the M^{2+} and M^{3+}cations on the overall frustration.

Conclusion

Several β-pyrochlores with the formula of $A_xM^{2+}{}_xM^{3+}{}_{(2-x)}F_6$ (A = Cs and Rb; M^{2+} = Co^{2+}, Ni^{2+} and Zn^{2+} and M^{3+} = V^{3+} and Fe^{3+}) were successfully synthesized using mild hydrothermal synthesis. $Rb(Zn_{0.2}V_{0.8})(Zn_{0.8}V_{0.2})F_6$ crystallizes with an orthorhombic structure, while all the other synthesized materials crystallize in cubic structures. The vanadium analogs $Cs_{0.86}Co_{0.86}V_{1.14}F_6$, $Cs_{0.9}Ni_{0.9}V_{1.1}F_6$, $Rb_{0.97}Ni_{0.97}V_{1.03}F_6$, and $Rb_{0.93}Co_{0.93}V_{1.07}F_6$ exhibit large Weiss temperatures that indicate dominant antiferromagnetic behavior in the materials, along with frustration indices between 6 – 13. Moreover, the dimensionless $C/(\chi|\theta_{CW}|) = T/|\theta_{CW}| - 1$ plot and the emergence of a hysteresis loop in the M vs. H plots for the compounds $Cs_{0.86}Co_{0.86}V_{1.1}F_6$ and $Rb_{0.93}Co_{0.93}V_{1.07}F_6$, indicate evidence of significant ferromagnetic interaction between Co^{2+} and V^{3+}, which appear to be more pronounced than those between Ni^{2+} and V^{3+}. Paramagnetic behavior was observed for $Cs_{0.9}Zn_{0.9}V_{1.1}F_6$ and $Rb(Zn_{0.2}V_{0.8})(Zn_{0.8}V_{0.2})F_6$ down to 2K, which highlights that the magnetic ordering of these compounds is disfavored when the M^{2+} cation lacks unpaired electrons. In contrast, $CsZnFeF_6$ exhibits a higher Weiss temperature compared to all vanadium analogs synthesized. Thus, we can suggest that all the nearest-neighbor magnetic interactions of $CsZnFeF_6$ are antiferromagnetic, which is further supported by the strong antiferromagnetic deviation in the $C/(\chi|\theta_{CW}|) = T/|\theta_{CW}| - 1$ plot. However, $CsZnFeF_6$ does not order magnetically above 2K. To determine the actual magnetic behavior of $CsZnFeF_6$ and to identify its magnetic structure will require a very low-temperature magnetic susceptibility study. Even though we can relate the effect of the M^{2+} and M^{3+} cations to the value of the Weiss temperature, there is still ambiguity surrounding how the magnetic ion's characteristics affect the frustration indices. Answering this question will require the synthesis and investigation of additional compounds of the pyrochlore family. However, we can infer that the frustration index is reduced in pyrochlores going from Fe^{3+} to Cr^{3+} to V^{3+}, and also when progressing from cubic pyrochlore to orthorhombic pyrochlore, and then to inverse weberite and weberite.

Acknowledgment

Financial support for this work was provided by the National Science Foundation via award DMR-2221403 and is gratefully acknowledged. We thank Dr. Perry J. Pellechia for assistance in the EPR

measurements and Dr. Juliano Schorne-Pinto and Dr. Mina Aziziha for assistance in the ICP-OES measurements.

Supporting Information

The Supporting Information is available free of charge at ???

Elemental composition data, crystal structure data, powder X-ray diffraction patterns, electronic paramagnetic resonance data, inductively coupled plasma optical emission spectroscopy (ICP-OES) data, and magnetic plots.

Accession Codes

CCDC 2258816–2258819, 2258952, 2258953 and 2258907 contain the supplementary crystallographic data for this paper. These data can be obtained free of charge *via* www.ccdc.cam.ac.uk/data_request/cif, or by emailing data_request@ccdc.cam.ac.uk, or by contacting The Cambridge Crystallographic Data Centre, 12 Union Road, Cambridge CB2 1EZ, UK; fax: +44 1223 336033.

References

1. Greedan, J. E. Geometrically Frustrated Magnetic Materials. *Funct. Oxide.* **2010**, *11*, 41-117.
2. Gardner, J. S.; Gingras, M. J. P.; Greedan, J. E. Magnetic Pyrochlore Oxides. *Rev. Mod. Phys.* **2010**, *82*, 53.
3. Greedan, J. E. Frustrated Rare Earth Magnetism: Spin Glasses, Spin Liquids and Spin Ices in Pyrochlore Oxides. *J. Alloys Compd.* **2006**, *408*, 444-455.
4. Reig-i-Plessis, D.; Hallas, A. M. Frustrated Magnetism in Fluoride and Chalcogenide Pyrochlore Lattice Materials. *Phys. Rev. Materials.* **2021**, *5*, 030301.
5. Fukazawa, H.; Maeno, Y. Magnetic Ground State of the Pyrochlore Oxide $Y_2Nb_2O_7$. *Phys. Rev. B.* **2003**, *67*, 054410.
6. Krizan, J. W.; Cava, R. J. $NaCaCo_2F_7$: A Single-Crystal High-Temperature Pyrochlore Antiferromagnet. *Phys. Rev. B.* **2014**, *89*, 214401.
7. Krizan, J. W.; Cava, R. J. $NaCaNi_2F_7$: A Frustrated High-Temperature Pyrochlore Antiferromagnet with S=1Ni^{2+}. *Phys. Rev. B.* **2015**, *92*, 014406.
8. Krizan, J. W.; Cava, R. J. $NaSrCo_2F_7$, A Co^{2+} Pyrochlore Antiferromagnet. *J. Phys.: Condens. Matter.* **2015**, *27*, 296002.
9. Sanders, M. B.; Krizan, J. W.; Plumb, K. W.; McQueen, T. M.; Cava, R. J. $NaSrMn_2F_7$, $NaCaFe_2F_7$, and $NaSrFe_2F_7$: Novel Single Crystal Pyrochlore Antiferromagnets. *J. Phys.: Condens. Matter.* **2017**, *29*, 045801.
10. Ramirez, A. P. Strongly Geometrically Frustrated Magnets. *Annu. Rev. Mater. Sci.* **1994**, *24*, 453-480.
11. Talanov, M. V.; Talanov, V. M. Formation of Breathing Pyrochlore Lattices: Structural, Thermodynamic and Crystal Chemical Aspects. *CrystEngComm.* **2020**, *22*, 1176-1187.
12. Anantharaman, A. P.; Dasari, H. P. Potential of Pyrochlore Structure Materials in Solid Oxide Fuel Cell Applications. *Ceram. Int.* **2021**, *47*, 4367-4388.
13. Jitta, R. R.; Gundeboina, R.; Veldurthi, N. K.; Guje, R.; Muga, V. Defect Pyrochlore Oxides: as Photocatalyst Materials for Environmental and Energy Applications - a review. *J. Chem. Technol. Biotechnol.* **2015**, *90*, 1937-1948.
14. Harris, M. J.; Zinkin, M. P. Frustration in the Pyrochlore Antiferromagnets. *Mod. Phys. Lett. B.* **1996**, *10*, 417-438.
15. Klepov, V. V.; Pace, K. A.; Berseneva, A. A.; Felder, J. B.; Calder, S.; Morrison, G.; Zhang, Q.; Kirkham, M. J.; Parker, D. S.; zur Loye, H.-C. Chloride Reduction of Mn^{3+} in Mild Hydrothermal Synthesis of a Charge Ordered Defect Pyrochlore, $CsMn^{2+}Mn^{3+}F_6$, a Canted Antiferromagnet with a Hard Ferromagnetic Component. *J. Am. Chem. Soc.* **2021**, *143*, 11554-11567.
16. Songvilay, M.; Rodriguez, E. E.; Lindsay, R.; Green, M. A.; Walker, H. C.; Rodriguez-Rivera, J. A.; Stock, C. Anharmonic Magnon Excitations in Noncollinear and Charge-Ordered $RbFe^{2+}Fe^{3+}F_6$. *Phys. Rev. Lett.* **2018**, *121*, 087201.
17. Alba, M.; Hammann, J.; Jacoboni, C.; Pappa, C. Very Low Field Susceptibility of the Highly Frustrated $CsMnFeF_6$ and $CsNiFeF_6$ Compounds. *Phys. Lett. A.* **1982**, *89*, 423-426.
18. Banks, E.; Deluca, J. A.; Berkooz, O. Preparation, Magnetic Properties and Mossbauer Study of the Modified Pyrochlores $M^{II}M^{III}F_6A$. *J. Solid State Chem.* **1973**, *6*, 569-573.
19. Enkler, D.; Roters, A.; Steiner, M. Low-field Magnetization in Compounds of the Modified Pyrochlore Structure $CsM_1{}^{2+}M^{3+}{}_2F_6$. *Solid State Commun.* **1994**, *92*, 481-484.

20. Kim, S. W.; Kim, S.-H.; Halasyamani, P. S.; Green, M. A.; Bhatti, K. P.; Leighton, C.; Das, H.; Fennie, C. J. $RbFe^{2+}Fe^{3+}F_6$: Synthesis, Structure, and Characterization of a New Charge-Ordered Magnetically Frustrated Pyrochlore-Related Mixed-Metal Fluoride. *Chem. Sci.* **2012**, *3*, 741-751.
21. Liu, S.; Xu, Y.; Cui, Y.; Wang, J.; Sun, K.; Yu, S.; Hao, X. Charge Ordering and Magnetic Frustration in $CsFe_2F_6$. *J. Phys.: Condens. Matter.* **2017**, *29*, 315501.
22. Zinkin, M. P.; Harris, M. J.; Zeiske, T. Short-range Magnetic Order in the Frustrated Pyrochlore Antiferromagnet $CsNiCrF_6$. *Phys. Rev. B.* **1997**, *56*, 11786-11790.
23. Wanklyn, B. M.; Wondre, F. R.; Garrard, B. J.; Cermak, J.; Davison, W. Flux Growth of Crystals of some Transition Metal Fluorides: Part 3 Pyrochlores and others. *J. Mater. Sci.* **1981**, *16*, 2303−2309.
24. Babel, D.; Pausewang, G.; Viebahn, W. The Structure of some Fluorides, Oxides and Oxyfluorides AMe_2X_6: The $RbNiCrF_6$ type. *Z. Naturforsch., B: Chem. Sci.* **1967**, *22*, 1219-1220.
25. Baum, E.; Dahlke, P.; Kaiser, V.; Molinier, M.; Schmidt, R. E.; Pebler, J.; Massa, W.; Babel, D. On the Crystal Structure of Pyrochlores: Mössbauer Spectra of Orthorhombic $CsFe_2F_6$ and X-Ray Single Crystal Studies of the Cubic Compounds $CsMgGaF_6$, $CsM^{II}V^{III}F_6$ (M^{II}= Mn, Zn), $CsM^{II}Fe^{III}F_6$ (M^{II}= Mn, Cu, Zn) and $Cs_4Cu_5V_3O_2F_{19}$. *Z. Anorg. Allg. Chem.* **2006**, *632*, 2244-2250.
26. Raju, K. S.; Wanklyn, B. M. Characterization of Modified Pyrochlores $CsMFeF_6$ (M= Mn, Co and Zn). *J. Cryst. Growth.* **1993**, *128*, 1078-1080.
27. APEX3 Version 2019.1-0 and SAINT+ Version 8.40A. **2019**.
28. Krause, L.; Herbst-Irmer, R.; Sheldrick, G. M.; Stalke, D. Comparison of Silver and Molybdenum Microfocus X-ray Sources for Single-Crystal Structure Determination. *J. Appl. Crystallogr.* **2015**, *48*, 3-10.
29. Sheldrick, G. M. SHELXT– Integrated Space-Group and Crystal-Structure Determination. *Acta Cryst. A.* **2015**, *71*, 3-8.
30. Morrison, G.; zur Loye, H.-C. Simple Correction for the Sample Shape and Radial Offset effects on SQUID Magnetometers: Magnetic Measurements on Ln_2O_3 (Ln=Gd, Dy, Er) Standards. *J. Solid State Chem.* **2015**, *221*, 334-337.
31. Ayer, G. B.; Klepov, V. V.; Pace, K. A.; zur Loye, H.-C. Quaternary Cerium(IV) Containing Fluorides Exhibiting Ce_3F_{16} Sheets and Ce_6F_{30} Frameworks. *Dalton Trans.* **2020**, *49*, 5898-5905.
32. Ayer, G. B.; Klepov, V. V.; Smith, M. D.; zur Loye, H.-C. Mild Hydrothermal Synthesis of the Complex Hafnium-Containing Fluorides $Cs_2[M(H_2O)_6][Hf_2F_{12}]$ (M = Ni, Co, Zn), $CuHfF_6(H_2O)_4$, and $Cs_2Hf_3Mn_3F_{20}$ Based on HfF_7 and HfF_6 Coordination Polyhedra. *Inorg. Chem.* **2019**, *58*, 13049-13057.
33. Keerthisinghe, N.; Berseneva, A. A.; Klepov, V. V.; Morrison, G.; zur Loye, H.-C. A Geometrically Frustrated Family of $M^{II}M^{III}F_5(H_2O)_2$ Mixed–Metal Fluorides with Complex Magnetic Interactions. *Inorg. Chem.* **2021**, *60*, 14318-14329.
34. Lal, S.; Pandey, S. K. Limitations of Unconstrained LSDA+ U Calculations in Predicting the Electronic and Magnetic Ground State of a Geometrically Frustrated ZnV_2O_4 Compound. *J. Magn. Magn. Mater.* **2016**, *412*, 23-29.
35. Shrivastava, V.; Tripathi, V. K.; Nagarajan, R. Implications of Including a Magnetic Ion (Cr^{3+} and Fe^{3+}) at the Vanadium Site in a Geometrically Frustrated Spinel MgV_2O_4: Magnetic and Catalytic Properties. *Dalton Trans.* **2019**, *48*, 16661-16670.

36. Mugiraneza, S.; Hallas, A. M. Tutorial: a Beginner's Guide to Interpreting Magnetic Susceptibility Data with the Curie-Weiss Law. *Commun. Phys.* **2022**, *5*, 95.
37. Kanamori, J. Superexchange Interaction and Symmetry Properties of Electron Orbitals. *J. Phys. Chem. Solids.* **1959**, *10*, 87-98.
38. Laligant, Y.; Calage, Y.; Torres-Tapia, E.; Greneche, J. M.; Varret, F.; Ferey, G. Crystal Structure of the Inverse Weberite $ZnFeF_5(H_2O)_2$, Magnetic and Mössbauer Study of the Antiferromagnet $ZnFeF_5(H_2O)_2$ and ferrimagnet $MnFeF_5(H_2O)_2$. *J. Magn. Magn. Mater.* **1986**, *61*, 283-290.
39. Laligant, Y.; Leblanc, M.; Pannetier, J.; Ferey, G. Ordered Magnetic Frustration. IV. The Two Magnetic Structures of the Inverse Weberite $Fe_2F_5(H_2O)_2$: an Example of the Thermal Evolution of the Frustration Character. *J. Phys. C: Solid State Phys.* **1986**, *19*, 1081.
40. Boireau, A.; Gravereau, P.; Dance, J. M.; Tressaud, A.; Hagenmuller, P.; Soubeyroux, J. L.; Welsch, M.; Babel, D. Structural and Magnetic Properties of Several Cobalt (II) Weberites. *Mater. Res. Bull.* **1993**, *28*, 27-38.
41. Cai, L.; Nino, J. C. Complex Ceramic Structures. I. Weberites. *Acta Crystallogr., Sect. B: Struct. Sci.* **2009**, *65*, 269-290.

For Table of Content Use Only

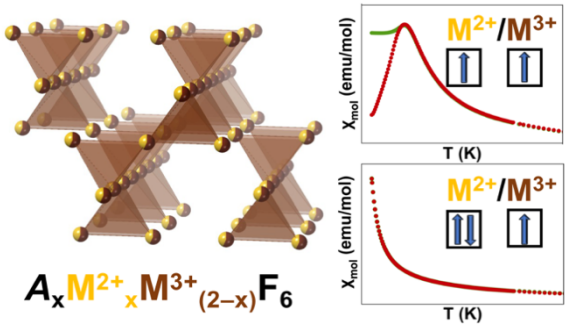

Conner sharing tetrahedra network of magnetic cations leads to the geometric magnetic frustration in β-pyrochlores. Seven novel nonstoichiometric β-pyrochlores have been synthesized *via* the hydrothermal method. A notable magnetic transition with prominent antiferromagnetic interactions can be observed at low temperatures when both cations have unpaired electrons. Frustration indices of those β-pyrochlores range between 6-13.